Joint Beamforming and Illumination Pattern Design for Beam-Hopping LEO Satellite Communications

Jing Wang, *Graduate Student Member, IEEE*, Chenhao Qi, *Senior Member, IEEE*, Shui Yu, *Fellow, IEEE*, and Shiwen Mao, *Fellow, IEEE*

***Abstract*— Since hybrid beamforming (HBF) can approach the performance of fully-digital beamforming (FDBF) with much lower hardware complexity, we investigate the HBF design for beam-hopping (BH) low earth orbit (LEO) satellite communications (SatComs). Aiming at maximizing the sum-rate of totally illuminated beam positions during the whole BH period, we consider joint beamforming and illumination pattern design subject to the HBF constraints and sum-rate requirements. To address the non-convexity of the HBF constraints, we temporarily replace the HBF constraints with the FDBF constraints. Then we propose an FDBF and illumination pattern random search (FDBF-IPRS) scheme to optimize illumination patterns and fully-digital beamformers using constrained random search and fractional programming methods. To further reduce the computational complexity, we propose an FDBF and illumination pattern alternating optimization (FDBF-IPAO) scheme, where we relax the integer illumination pattern to continuous variables and after finishing all the iterations we quantize the continuous variables into integer ones. Based on the fully-digital beamformers designed by the FDBF-IPRS or FDBF-IPAO scheme, we propose an HBF alternating minimization algorithm to design the hybrid beamformers. Simulation results show that the proposed schemes can achieve satisfactory sum-rate performance for BH LEO SatComs.**

***Index Terms*— Beam-hopping (BH), hybrid beamforming (HBF), illumination pattern, LEO satellite communications.**

I. Introduction

TO ACHIEVE full coverage of spatial and terrestrial wireless communications, the upcoming sixth generation wireless communications integrating satellite communications (SatComs) will establish a fully connected wireless network. SatComs can provide seamless and stable wireless service to complement and extend terrestrial communications, and therefore can address the challenge of insufficient connectivity for remote areas such as deserts, mountains and oceans [2], [3], [4]. Compared to medium earth orbit and geosynchronous earth orbit counterparts, the low earth orbit (LEO) satellites are proximal to the earth, with the advantages of low latency in wireless access, reduced energy for launching, and small power for signal transmission from the satellites to terrestrial receivers [5]. Therefore, LEO SatComs have received increasing attention and become hotspots of commercial investment. The companies such as SpaceX and Amazon, have already put forward their commercial LEO SatCom products including Starlink and Kuiper [6].

As one of the key technologies of LEO SatComs, beam-hopping (BH) has raised great interest from both academia and the industry, owing to its flexibility and low complexity for implementation [5], [7]. BH is capable of achieving multi-beam coverage with reduced inter-beam interference [8], [9] and improved resource utilization [10], [11], by simultaneously activating a set of beams at each time slot in a designed illumination pattern and periodically repeating in the next BH time window. To reduce the inter-beam interference among illuminated beams in the same time slot, adjacent beams are not preferred by the BH [8]. Aiming at minimizing the interference-based penalty function, a dynamic BH scheme is proposed in conjunction with selective precoding [9]. To appropriately allocate the resource in SatComs, a joint power allocation and BH design scheme with non-orthogonal multiple access is employed subject to the requested traffic demands [10]. Aiming at efficiently utilizing time domain and power domain resources in BH SatComs, an adaptive resource adjustment method is proposed to design the BH illumination pattern and transmit power allocation [11].

Furthermore, the beamforming has been widely adopted to achieve high data-rate for LEO SatComs. Aiming at maximizing the sum-rate of the SatCom system, a joint beamforming and power allocation scheme is proposed to mitigate the interference among the ground users [12]. Compared to the fully-digital beamforming (FDBF) that achieves the satisfactory performance at the cost of very-high hardware complexity [13], [14], hybrid beamforming (HBF) is promising to balance the performance and hardware constraints. A hybrid analog and digital beamforming method is

Received 31 March 2024; revised 20 July 2024; accepted 15 September 2024. Date of publication 25 September 2024; date of current version 12 December 2024. The work of Jing Wang and Chenhao Qi was supported in part by the National Key Research and Development Program of China under Grant 2021YFB2900404 and in part by the National Natural Science Foundation of China under Grant 62071116 and Grant U22B2007. The work of Shiwen Mao was supported in part by the National Science Foundation under Grant CNS-2415208. An earlier version of this paper was presented in part at the IEEE Global Communications Conference, Kuala Lumpur, Malaysia, December 2023 [DOI: 10.1109/GLOBECOM54140.2023.10436908]. The associate editor coordinating the review of this article and approving it for publication was Y. Shi. *(Corresponding author: Chenhao Qi.)*

Jing Wang and Chenhao Qi are with the School of Information Science and Engineering, Southeast University, Nanjing 210096, China (e-mail: wangjing12@seu.edu.cn; qch@seu.edu.cn).

Shui Yu is with the Faculty of Engineering and Information Technology, University of Technology Sydney, Sydney, NSW 2007, Australia (e-mail: Shui.Yu@uts.edu.au).

Shiwen Mao is with the Department of Electrical and Computer Engineering, Auburn University, Auburn, AL 36849 USA (e-mail: smao@ieee.org).

Color versions of one or more figures in this article are available at https://doi.org/10.1109/TWC.2024.3463002.

Digital Object Identifier 10.1109/TWC.2024.3463002

developed in the massive MIMO LEO SatCom systems [15], where the HBF architecture is equipped at the satellite to transmit multiple beams. To further mitigate intra-beam and inter-beam interference, a two-stage HBF scheme together with an adaptive user scheduling scheme is proposed for millimeter-wave spectrum coexisting integrated terrestrial-satellite network [16]. Based on the angel information instead of channel state information in SatComs, an HBF scheme is designed using the codebook to perform the beam selection for the LEO SatComs [17]. To achieve flexible beam coverage while maintaining the RF cost for the LEO SatComs, the beamforming based on movable antenna array is considered with the time-varying beam coverage for terrestrial users [18], [19].

By combining the advantages of the flexibility and high data-rate, the beamforming design is considered for SatComs with BH. To reduce the power consumption, compressed sensing is employed to design FDBF with BH [8]. To balance the data traffic among clusters where each cluster is formed by multiple beams, a joint optimization method of singular-value-decomposition FDBF and BH is proposed subject to the service requirement of each beam [20]. Aiming at maximizing the energy efficiency in BH SatComs, a cluster-based BH scheme with FDBF design is proposed to achieve the on-demand capacity allocation [21]. However, to the best knowledge of authors, so far there has been no work on HBF for LEO SatComs with BH aiming at sum-rate maximization. Note that the sum-rate maximization is an important objective for wireless communications including SatComs and the HBF can effectively reduce the hardware complexity for the payload of the satellite.

In this paper, we investigate the HBF design for BH SatComs. Aiming at maximizing the sum-rate of totally illuminated beam positions during the whole BH period, we consider joint beamforming and illumination pattern (BIP) design subject to the HBF constraints and sum-rate requirements. As a summary, our contributions include the following three points, where the first point is included in our conference paper [1].

- To address the non-convexity of the HBF constraints, we temporarily replace the HBF constraints with the FDBF constraints. Then an FDBF and illumination pattern random search (FDBF-IPRS) scheme is proposed, where the illumination pattern of SatComs is generated by the constrained random search and then the fully-digital beamformers of the satellite are designed by the fractional programming (FP) methods.
- To reduce the computational complexity, we propose an FDBF and illumination pattern alternating optimization (FDBF-IPAO) scheme to decouple the BIP problem into two subproblems, namely, the FDBF design subproblem and the illumination pattern design subproblem, and alternately optimize these two subproblems until a stop condition is triggered. For the FDBF design subproblem, the FP method is employed to obtain the fully-digital beamformers. For the illumination pattern design subproblem that is mixed-integer and non-convex, we relax the integer illumination pattern to continuous variables so that the FP method can be used for the optimization. Once the stop condition is triggered, we quantize the continuous variables into integer ones to determine the illumination pattern.
- Based on the fully-digital beamformers designed by the FDBF-IPRS or FDBF-IPAO scheme, we propose an HBF alternating minimization (HBF-AM) algorithm to design the hybrid beamformers. By minimizing the Euclidean distance between the designed fully-digital beamformers and the hybrid beamformers, the digital beamformers and analog beamformers are iteratively optimized using the Riemannian manifold optimization method.

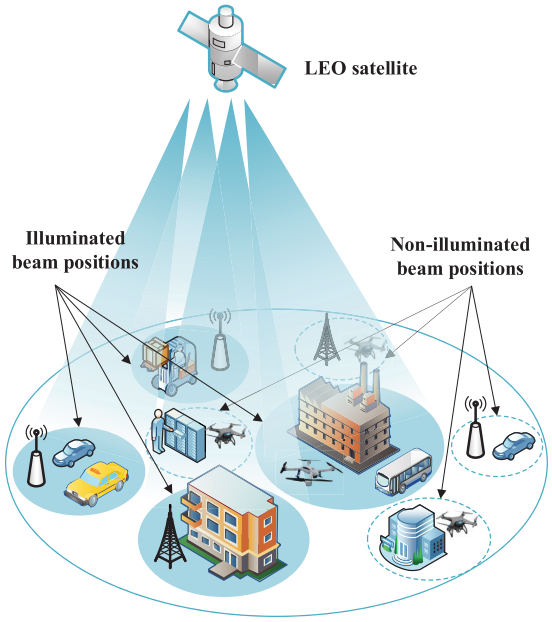

Fig. 1. Illustration of system model.

Notations: Boldfaced lowercase and uppercase letters represent vectors and matrices, respectively. The conjugate, expectation, transpose, Hermitian transpose, Frobenius norm, and Kronecker product are denoted as $(\cdot)^*$, $\mathbb{E}(\cdot)$, $(\cdot)^{\mathrm{T}}$, $(\cdot)^{\mathrm{H}}$, $\|\cdot\|_2$, and $\otimes$, respectively. $\mathbb{C}$ and $\mathbb{R}$ represent the sets of complex-valued numbers and real-valued numbers, respectively. $\boldsymbol{I}_{N_\mathrm{s}}$ denotes the Identity matrix with the dimension of $N_\mathrm{s} \times N_\mathrm{s}$. $\mathcal{M} \triangleq \{1, 2, \ldots, M\}$, $\mathcal{N} \triangleq \{1, 2, \ldots, N_\mathrm{s}\}$ and $\mathcal{N}_{\mathrm{BS}} \triangleq \{1, 2, \ldots, N_{\mathrm{BS}}\}$.

II. System Model

Consider a downlink LEO SatCom system, where the LEO satellite equipped with N_{BS} antennas can simultaneously generate K spot beams to illuminate K beam positions on the ground. To illuminate the total N_s beam positions, we use the BH, where each BH period includes M time slots. To guarantee that each beam position is illuminated at least once during each BH period, we require

$$KM \geqslant N_\mathrm{s}. \tag{1}$$

As illustrated in Fig. 1, the beam positions with different radius are determined according to the number of ground users and

the service demand before performing the BH [22]. Note that the satellite works in the multicast mode and therefore different users located in the same beam position receive the same signal from the satellite.

To transmit K independent data streams at each time slot, the LEO satellite employs the HBF architecture equipped with N_{RF} RF chains, where $K \leqslant N_{\mathrm{RF}}$. The HBF architecture includes analog beamformer $\boldsymbol{F}_t \in \mathbb{C}^{N_{\mathrm{BS}} \times N_{\mathrm{RF}}}$ and digital beamformer $\boldsymbol{Q}_t \in \mathbb{C}^{N_{\mathrm{RF}} \times N_{\mathrm{s}}}$ for the tth time slot, respectively. Let $\boldsymbol{s} \in \mathbb{C}^{N_{\mathrm{s}}}$ denote a symbol vector transmitted by the LEO satellite. The received signal at the total N_{s} beam positions in the tth time slot can be expressed as

$$\boldsymbol{y}_t = \boldsymbol{H}\boldsymbol{F}_t\boldsymbol{Q}_t\boldsymbol{s} + \boldsymbol{z},\ t \in \mathcal{M}, \tag{2}$$

where $\boldsymbol{z} \in \mathbb{C}^{N_{\mathrm{s}}}$ denotes an additive white Gaussian noise vector with $[\boldsymbol{z}]_n \sim \mathcal{CN}\left(0, \sigma^2\right)$, and $\boldsymbol{H} \in \mathbb{C}^{N_{\mathrm{s}} \times N_{\mathrm{BS}}}$ denotes the downlink SatCom channel matrix. Note that $\boldsymbol{H}$ is supposed to be the same during the whole BH period [9]. In fact, we have

$$\boldsymbol{H} \triangleq [\boldsymbol{h}_1^{\mathrm{T}}, \boldsymbol{h}_2^{\mathrm{T}}, \ldots, \boldsymbol{h}_{N_{\mathrm{s}}}^{\mathrm{T}}]^{\mathrm{T}}, \tag{3}$$

where $\boldsymbol{h}_n$ denotes the channel vector between the LEO satellite and the nth beam position for $n \in \mathcal{N}$. Assuming that the Doppler frequency shift caused by the satellite movement is compensated by the ground users and the sky is clear so that the rain attenuation is neglected, we can express $\boldsymbol{h}_n$ as

$$\boldsymbol{h}_n = \sum\nolimits_{l=1}^{L_n} g_l^{(n)} \boldsymbol{v}^{\mathrm{H}}\left(N_{\mathrm{BS}}, \theta_l^{(n)}\right), \tag{4}$$

where L_n denotes the number of the channel paths, $\theta_l^{(n)}$ represents the angle-of-departure of the lth channel path, and $\boldsymbol{v}\left(N_{\mathrm{BS}}, \theta_l^{(n)}\right)$ denotes the channel steering vector of a uniform linear array given as

$$\boldsymbol{v}\left(N_{\mathrm{BS}}, \theta_l^{(n)}\right) = \frac{1}{\sqrt{N_{\mathrm{BS}}}}\left[1, e^{j\pi\theta_l^{(n)}}, \ldots, e^{j\pi(N_{\mathrm{BS}}-1)\theta_l^{(n)}}\right]^{\mathrm{T}}, \tag{5}$$

for $l = 1, 2, \ldots, L_n$. In fact, we have $\theta_l^{(n)} = 2d_0\frac{f_{\mathrm{c}}}{v_{\mathrm{c}}}\sin\tilde{\theta}_l^{(n)}$, where d_0, f_{c} and v_{c} represent the antenna spacing, carrier frequency and speed of light, respectively, and $\tilde{\theta}_l^{(n)}$ denotes the physical angle of the lth channel path for $l = 1, 2, \ldots, L_n$. Note that $g_l^{(n)}$ represents the channel gain of the lth channel path obeying Rician fading distribution with Rician factor $\chi_l^{(n)}$ and $\mathbb{E}\left(\left|g_l^{(n)}\right|^2\right) = \eta_l^{(n)}$. Specifically, $\eta_l^{(n)}$ can be expressed as

$$\eta_l^{(n)} = \left(\frac{v_{\mathrm{c}}}{4\pi f_{\mathrm{c}} d}\right)^2 \frac{G_{\mathrm{r}} G_{\mathrm{t}} N_{\mathrm{BS}}}{\kappa B T_{\mathrm{R}}}, \tag{6}$$

where B, d, κ, and T_{R} represent the bandwidth, propagation distance, Boltzmann's constant and receiving noise temperature, respectively. G_{r} and G_{t} denote the transmitting antenna gain of the satellite and receiving antenna gain of the ground users, respectively [15].

We denote a binary variable $x_{n,t} \in \{0, 1\}$ as the illumination indicator of the nth beam position in the tth time slot, for $t \in \mathcal{M}$ and $n \in \mathcal{N}$. If $x_{n,t} = 1$, the nth beam position is illuminated by a spot beam of the LEO satellite at the tth time slot; otherwise, it is not illuminated. Since the LEO satellite can simultaneously generate at most K spot beams in each time slot, we have

$$\sum\nolimits_{n=1}^{N_{\mathrm{s}}} x_{n,t} \leqslant K. \tag{7}$$

We define the illumination pattern as $\boldsymbol{X}$, where

$$[\boldsymbol{X}]_{n,t} \triangleq x_{n,t},\ n \in \mathcal{N},\ t \in \mathcal{M}. \tag{8}$$

To simplify the notation, we define

$$\boldsymbol{Q}_t \triangleq [\boldsymbol{q}_1^t, \boldsymbol{q}_2^t, \ldots, \boldsymbol{q}_{N_{\mathrm{s}}}^t]. \tag{9}$$

Then, the achievable rate of the nth beam position in the tth time slot can be expressed as

$$R_{n,t}\left(\boldsymbol{F}_t, \boldsymbol{Q}_t, \boldsymbol{X}\right) = \log_2\left(1 + \frac{x_{n,t}\left|\boldsymbol{h}_n\boldsymbol{F}_t\boldsymbol{q}_n^t\right|^2}{\sum_{k\neq n}^{N_{\mathrm{s}}} x_{k,t}\left|\boldsymbol{h}_n\boldsymbol{F}_t\boldsymbol{q}_k^t\right|^2 + \sigma^2}\right). \tag{10}$$

III. Joint Beamforming and Illumination Pattern Design

To maximize the sum-rate of the total N_{s} beam positions during the whole BH period, we jointly optimize the analog and digital beamforming matrices $\{\boldsymbol{F}_t, \boldsymbol{Q}_t, t \in \mathcal{M}\}$ together with the illumination pattern. The joint BIP design problem can be formulated as

$$\max_{\boldsymbol{X}, \{\boldsymbol{F}_t, \boldsymbol{Q}_t, t\in\mathcal{M}\}} \sum_{n=1}^{N_{\mathrm{s}}}\sum_{t=1}^{M} R_{n,t}\left(\boldsymbol{F}_t, \boldsymbol{Q}_t, \boldsymbol{X}\right) \tag{11a}$$

$$\text{s.t.} \quad \sum_{t=1}^{M} R_{n,t}\left(\boldsymbol{F}_t, \boldsymbol{Q}_t, \boldsymbol{X}\right) \geqslant \gamma_n, \forall n \in \mathcal{N}, \tag{11b}$$

$$\sum_{n=1}^{N_{\mathrm{s}}} \left\|\boldsymbol{F}_t\boldsymbol{q}_n^t\right\|_2^2 \leqslant P_{\mathrm{tot}}, \forall t \in \mathcal{M}, \tag{11c}$$

$$\left|[\boldsymbol{F}_t]_{i,n}\right| = 1, \forall i \in \mathcal{N}_{\mathrm{BS}}, n \in \mathcal{N}, \tag{11d}$$

$$\sum\nolimits_{n=1}^{N_{\mathrm{s}}} x_{n,t} \leqslant K, \forall t \in \mathcal{M}, \tag{11e}$$

$$x_{n,t} \in \{0, 1\}, \forall n \in \mathcal{N}, \forall t \in \mathcal{M}, \tag{11f}$$

where γ_n and P_{tot} are the predefined threshold of the sum-rate and the power constraint, respectively. To be specific, constraint (11b) indicates that the sum-rate of the nth beam position during the whole BH period is no smaller than γ_n. Constraint (11c) indicates that the total transmit power of the LEO satellite in each time slot is no larger than P_{tot}. Constraint (11d) indicates the unit-modulus constraints of analog beamformers. Constraint (11e) indicates that the maximum number of illuminated beam positions in each time slot is no larger than K. In fact, the constraints (11c), (11d) and (11e) compose the HBF constraints.

It is seen from (11a) and (11b) that the beamforming matrices and the illumination pattern are coupled, leading (11) to be a mixed integer non-convex optimization problem. To solve this joint BIP design problem, we temporarily replace the HBF constraints with the FDBF constraints and then design the illumination pattern.

Define the fully-digital beamformer at the tth time slot for $t \in \mathcal{M}$ as

$$\boldsymbol{P}_t \triangleq [\boldsymbol{p}_1^t, \boldsymbol{p}_2^t, \ldots, \boldsymbol{p}_{N_\mathrm{s}}^t] \in \mathbb{C}^{N_{\mathrm{BS}} \times N_\mathrm{s}}. \tag{12}$$

We temporarily replace the HBF constraints on $\boldsymbol{F}_t$ and $\boldsymbol{Q}_t$, with the FDBF constraints on $\boldsymbol{P}_t$. Then the fully-digital BIP design problem can be given as

$$\max_{\boldsymbol{X}, \{\boldsymbol{P}_t, t\in\mathcal{M}\}} \sum_{n=1}^{N_\mathrm{s}} \sum_{t=1}^{M} R_{n,t}\left(\boldsymbol{P}_t, \boldsymbol{X}\right) \tag{13a}$$

$$\text{s.t.} \quad \sum_{t=1}^{M} R_{n,t}\left(\boldsymbol{P}_t, \boldsymbol{X}\right) \geqslant \gamma_n, \forall n \in \mathcal{N}, \tag{13b}$$

$$\sum_{n=1}^{N_\mathrm{s}} \left\|\boldsymbol{p}_n^t\right\|_2^2 \leqslant P_{\mathrm{tot}}, \forall t \in \mathcal{M}, \tag{13c}$$

$$(11e), (11f), \tag{13d}$$

which is also a mixed integer non-convex optimization problem.

To solve (13), we propose the FDBF-IPRS and FDBF-IPAO schemes in Section III-A and Section III-B, respectively. For the FDBF-IPRS scheme, the illumination pattern of SatComs is generated by the constrained random search and then the fully-digital beamformers of the satellite are designed by the FP methods. For the FDBF-IPAO scheme, we decouple the fully-digital BIP problem into two subproblems, namely, the FDBF design subproblem and the illumination pattern design subproblem, and alternately optimize these two subproblems until a stop condition is triggered. For the FDBF design subproblem, the FP method is employed to obtain the fully-digital beamformers. For the illumination pattern design subproblem that is mixed-integer and non-convex, we relax the integer illumination pattern to continuous variables so that the FP method can be used for the optimization. Once the stop condition is triggered, we quantize the continuous variables into integer ones to determine the illumination pattern.

To solve (11), in Section III-C we propose an HBF-AM algorithm to design the hybrid beamformers based on the fully-digital beamformers designed by the FDBF-IPRS or FDBF-IPAO scheme. By minimizing the Euclidean distance between the designed fully-digital beamformers and the hybrid beamformers, the digital beamformers and analog beamformers are iteratively optimized using the Riemannian manifold optimization method.

A. FDBF-IPRS Scheme

Suppose the candidate illumination patterns are denoted by a set $\{\mathcal{X}_i, i \in \mathcal{I}\}$, where I is the number of candidate illumination pattern sets and $\mathcal{I} \triangleq \{1, 2, \ldots, I\}$. To reduce the complexity of exhaustive search, we generate $\{\mathcal{X}_i, i \in \mathcal{I}\}$ obeying the following two criteria.

- To completely utilize the resource in each time slot, we simultaneously illuminated K beams in the tth time slot, i.e., replacing the inequality by the equality in (11e) as

$$\sum_{n=1}^{N_\mathrm{s}} x_{n,t} = K, \ \forall t \in \mathcal{M}. \tag{14}$$

- To avoid the redundant illumination, the nth beam position can only be illuminated once during the whole BH period, which can be expressed as

$$\sum_{t=1}^{M} x_{n,t} = 1, \ \forall n \in \mathcal{N}. \tag{15}$$

The index set of non-illuminated beam positions at the tth time slot, denoted as $\mathcal{B}$, is initialized to be $\mathcal{N}$. The index set of illuminated beam positions at the tth time slot, denoted as $\mathcal{A}_t$, is determined by randomly choosing K beam positions from $\mathcal{B}$. At the next time slot, we update $\mathcal{B}$ by removing the beam positions of $\mathcal{A}_t$ from $\mathcal{B}$, which can be expressed as

$$\mathcal{B} \leftarrow \mathcal{B} \backslash \mathcal{A}_t. \tag{16}$$

By repeating (16), we determine $\mathcal{A}_t$ for $t = 1, 2, \ldots, M$. Then we can determine $\boldsymbol{X}$ by

$$x_{n,t} = \begin{cases} 1, & n \in \mathcal{A}_t, t \in \mathcal{M} \\ 0, & \text{otherwise} \end{cases}. \tag{17}$$

Since $\boldsymbol{X}$ satisfies (14) and (15), it is a valid candidate illumination pattern, which can be added to $\{\mathcal{X}_i, i \in \mathcal{I}\}$ by

$$\mathcal{X}_i \leftarrow \boldsymbol{X}, i \in \mathcal{I}. \tag{18}$$

In this way, we can determine $\{\mathcal{X}_i, i \in \mathcal{I}\}$, which is essentially based on the constrained random search. In the following, based on the candidate illumination patterns, we will find one achieving the largest sum-rate.

Given $\boldsymbol{X} = \mathcal{X}_i, i \in \mathcal{I}$, the FDBF design subproblem of (13) can be rewritten as

$$\max_{\{\boldsymbol{P}_t, t\in\mathcal{M}\}} \sum_{n=1}^{N_\mathrm{s}} \sum_{t=1}^{M} R_{n,t}\left(\boldsymbol{P}_t, \boldsymbol{X}\right) \tag{19a}$$

$$\text{s.t.} \quad \sum_{t=1}^{M} R_{n,t}\left(\boldsymbol{P}_t, \boldsymbol{X}\right) \geqslant \gamma_n, \forall n \in \mathcal{N}, \tag{19b}$$

$$\sum_{n=1}^{N_\mathrm{s}} \left\|\boldsymbol{p}_n^t\right\|_2^2 \leqslant P_{\mathrm{tot}}, \forall t \in \mathcal{M}, \tag{19c}$$

which is non-convex due to the logarithmic-fractional form of the objective function (19a) and constraint (19b). To deal with the non-convexity of (19), the FP method can be applied using the quadratic transform [23]. To simplify the notation, we define

$$\widehat{\boldsymbol{P}}_k^t \triangleq \boldsymbol{p}_k^t \left(\boldsymbol{p}_k^t\right)^{\mathrm{H}}, k \in \mathcal{N}. \tag{20}$$

Then (19) can be transformed into

$$\max_{\substack{\{\boldsymbol{P}_t, t\in\mathcal{M}\}, \\ \{\mu_{n,t}, t\in\mathcal{M}, n\in\mathcal{N}\}}} \sum_{n=1}^{N_\mathrm{s}} \sum_{t=1}^{M} f_{n,t}\left(\boldsymbol{p}_n^t, \mu_{n,t}\right) \tag{21a}$$

Algorithm 1 FDBF-IPRS Scheme

Input: N_{s}, N_{BS}, K, M and I.
Initialization: $\mathcal{B} \leftarrow \mathcal{N}$.
for $i = 1, 2, \ldots, I$ **do**
  for $t = 1, 2, \ldots, M$ **do**
    Determine $\mathcal{A}_t$ based on $\mathcal{B}$.
    Update $\mathcal{B}$ via (16).
  end for
  Obtain $\mathcal{X}_i$ via (18).
  repeat
    Update $\{\mu_{n,t}, t \in \mathcal{M}, n \in \mathcal{N}\}$ via (23).
    Obtain $\{\boldsymbol{P}_t, t \in \mathcal{M}\}$ by solving (19).
  until *Stop Condition 1* is triggered
  Obtain $\overline{\boldsymbol{P}}_1^{(i)}, \overline{\boldsymbol{P}}_2^{(i)}, \ldots, \overline{\boldsymbol{P}}_M^{(i)}$ via (26).
end for
Obtain $[\widetilde{\boldsymbol{P}}_1, \widetilde{\boldsymbol{P}}_2, \ldots, \widetilde{\boldsymbol{P}}_M, \widetilde{\boldsymbol{X}}]$ via (27).
Output: $\widetilde{\boldsymbol{P}}_1, \widetilde{\boldsymbol{P}}_2, \ldots, \widetilde{\boldsymbol{P}}_M$ and $\widetilde{\boldsymbol{X}}$.

$$\text{s.t.} \quad \sum_{t=1}^{M} f_{n,t}\left(\boldsymbol{p}_n^t, \mu_{n,t}\right) \geqslant \gamma_n, \forall n \in \mathcal{N}, \tag{21b}$$

$$(19c). \tag{21c}$$

Note that a new function $f_{n,t}\left(\boldsymbol{p}_n^t, \mu_{n,t}\right)$ in (21) is defined as

$$f_{n,t}\left(\boldsymbol{p}_n^t, \mu_{n,t}\right) \triangleq \log_2\Big(1 + 2\mathrm{Re}\left\{\sqrt{x_{n,t}}\mu_{n,t}^{\mathrm{H}}\boldsymbol{h}_n\boldsymbol{p}_n^t\right\} - \mu_{n,t}^{\mathrm{H}}\Big(\sum\nolimits_{k\neq n}^{N_{\mathrm{s}}} x_{k,t}\boldsymbol{h}_n\widehat{\boldsymbol{P}}_k^t\boldsymbol{h}_n^{\mathrm{H}} + \sigma^2\Big)\mu_{n,t}\Big), \tag{22}$$

where an auxiliary variable $\mu_{n,t}$ is defined as

$$\mu_{n,t} \triangleq \frac{\sqrt{x_{n,t}}\boldsymbol{h}_n\boldsymbol{p}_n^t}{\sum_{k\neq n}^{N_{\mathrm{s}}} x_{k,t}\boldsymbol{h}_n\widehat{\boldsymbol{P}}_k^t\boldsymbol{h}_n^{\mathrm{H}} + \sigma^2}. \tag{23}$$

In fact, $\mu_{n,t}$ is determined by setting

$$\frac{\partial f_{n,t}\left(\boldsymbol{p}_n^t, \mu_{n,t}\right)}{\partial \mu_{n,t}} = 0. \tag{24}$$

Note that with fixed $\{\mu_{n,t}, t \in \mathcal{M}, n \in \mathcal{N}\}$, (21) is convex, which is equivalent to (19) and can be solved by the interior-point method. By alternately updating $\{\mu_{n,t}, t \in \mathcal{M}, n \in \mathcal{N}\}$ with fixed $\{\boldsymbol{P}_t, t \in \mathcal{M}\}$ and updating $\{\boldsymbol{P}_t, t \in \mathcal{M}\}$ with fixed $\{\mu_{n,t}, t \in \mathcal{M}, n \in \mathcal{N}\}$, we run the iteration until triggering *Stop Condition 1*, which can be set as the maximum iteration number being reached. Then we can obtain a solution of $\boldsymbol{p}_n^t$ as

$$\overline{\boldsymbol{p}}_n^t = \arg\max_{\boldsymbol{p}_n^t} \sum_{n=1}^{N_{\mathrm{s}}}\sum_{t=1}^{M} f_{n,t}\left(\boldsymbol{p}_n^t, \mu_{n,t}\right). \tag{25}$$

Therefore, given $\mathcal{X}_i, i \in \mathcal{I}$, we can obtain $\overline{\boldsymbol{p}}_n^t$, $t = 1, 2, \ldots, M$, based on the procedures from (19) to (25). Then the designed beamforming matrix given $\mathcal{X}_i$ is denoted as

$$\overline{\boldsymbol{P}}_t^{(i)} \triangleq [\overline{\boldsymbol{p}}_1^t, \overline{\boldsymbol{p}}_2^t, \ldots, \overline{\boldsymbol{p}}_{N_{\mathrm{s}}}^t]. \tag{26}$$

Then the optimized $\widetilde{\boldsymbol{X}}$ together with the designed FDBF matrices $\widetilde{\boldsymbol{P}}_1, \widetilde{\boldsymbol{P}}_2, \ldots, \widetilde{\boldsymbol{P}}_M$ can be obtained by

$$[\widetilde{\boldsymbol{P}}_1, \widetilde{\boldsymbol{P}}_2, \ldots, \widetilde{\boldsymbol{P}}_M, \widetilde{\boldsymbol{X}}] = \arg\max_{\left\{\overline{\boldsymbol{P}}_1^{(i)}, \overline{\boldsymbol{P}}_2^{(i)}, \ldots, \overline{\boldsymbol{P}}_M^{(i)}, \mathcal{X}_i, i\in\mathcal{I}\right\}} \sum_{n=1}^{N_{\mathrm{s}}}\sum_{t=1}^{M} R_{n,t}\left(\overline{\boldsymbol{P}}_t^{(i)}, \mathcal{X}_i\right), \tag{27}$$

which achieves the largest sum-rate.

The detailed steps of the proposed FDBF-IPRS scheme are summarized in **Algorithm 1**. The computational complexity of the FDBF-IPRS scheme is $O\left(IT_1(MN_{\mathrm{BS}}N_{\mathrm{s}})^{3.5}\log_2(1/\varepsilon_1)\right)$, where T_1 denotes the predefined maximum iteration number of *Stop Condition 1* and $\varepsilon_1 > 0$ is the solution accuracy of the CVX solver used in the FDBF-IPRS scheme [24].

B. FDBF-IPAO Scheme

Due to the binary property of $\boldsymbol{X}$, (13) is a mixed integer non-convex optimization problem, which is difficult to solve. To reduce the difficulty in tackling integer variables, we relax the binary variable $x_{n,t}$ to a continuous variable $\widehat{x}_{n,t}$, with $0 \leqslant \widehat{x}_{n,t} \leqslant 1$, and then transform (13) into a continuous optimization problem. In fact, we will quantize the continuous variables into binary ones after finishing all the iterations.

To solve (13), we decouple it into two subproblems, namely, the FDBF design subproblem and the illumination pattern design subproblem, and alternately optimize these two subproblems until a stop condition is triggered.

Define $[\widehat{\boldsymbol{X}}]_{n,t} \triangleq \widehat{x}_{n,t}$, $n \in \mathcal{N}$, $t \in \mathcal{M}$. For the FDBF design subproblem, given $\widehat{\boldsymbol{X}}$, (13) can be rewritten as

$$\max_{\{\boldsymbol{P}_t, t\in\mathcal{M}\}} \sum_{n=1}^{N_{\mathrm{s}}}\sum_{t=1}^{M} R_{n,t}\left(\boldsymbol{P}_t, \widehat{\boldsymbol{X}}\right) \tag{28a}$$

$$\text{s.t.} \quad \sum_{t=1}^{M} R_{n,t}\left(\boldsymbol{P}_t, \widehat{\boldsymbol{X}}\right) \geqslant \gamma_n, \forall n \in \mathcal{N}, \tag{28b}$$

$$\sum_{n=1}^{N_{\mathrm{s}}} \left\|\boldsymbol{p}_n^t\right\|_2^2 \leqslant P_{\mathrm{tot}}, \forall t \in \mathcal{M}, \tag{28c}$$

which is non-convex due to the logarithmic-fractional form of the objective function (28a) and constraint (28b). To deal with the non-convexity of (28), the FP method can be applied using the quadratic transform [23]. Then (28) can be transformed into

$$\max_{\substack{\{\boldsymbol{P}_t, t\in\mathcal{M}\},\\ \{\zeta_{n,t}, t\in\mathcal{M}, n\in\mathcal{N}\}}} \sum_{n=1}^{N_{\mathrm{s}}}\sum_{t=1}^{M} f_{n,t}\left(\boldsymbol{p}_n^t, \zeta_{n,t}\right) \tag{29a}$$

$$\text{s.t.} \quad \sum_{t=1}^{M} f_{n,t}\left(\boldsymbol{p}_n^t, \zeta_{n,t}\right) \geqslant \gamma_n, \forall n \in \mathcal{N}, \tag{29b}$$

$$(28c). \tag{29c}$$

Note that a new function $f_{n,t}\left(\boldsymbol{p}_n^t, \zeta_{n,t}\right)$ in (29) is defined as

$$f_{n,t}\left(\boldsymbol{p}_n^t, \zeta_{n,t}\right) \triangleq \log_2\Big(1 + 2\mathrm{Re}\left\{\sqrt{\widehat{x}_{n,t}}\zeta_{n,t}^{\mathrm{H}}\boldsymbol{h}_n\boldsymbol{p}_n^t\right\} - \zeta_{n,t}^{\mathrm{H}}\Big(\sum\nolimits_{k\neq n}^{N_{\mathrm{s}}} \widehat{x}_{k,t}\boldsymbol{h}_n\widehat{\boldsymbol{P}}_k^t\boldsymbol{h}_n^{\mathrm{H}} + \sigma^2\Big)\zeta_{n,t}\Big), \tag{30}$$

where an auxiliary variable $\zeta_{n,t}$ is defined as

$$\zeta_{n,t} \triangleq \frac{\sqrt{\widehat{x}_{n,t}}\boldsymbol{h}_n\boldsymbol{p}_n^t}{\sum_{k\neq n}^{N_s}\widehat{x}_{k,t}\boldsymbol{h}_n\widehat{\boldsymbol{P}}_k^t\boldsymbol{h}_n^{\mathrm{H}}+\sigma^2}. \tag{31}$$

In fact, $\zeta_{n,t}$ is determined by setting

$$\frac{\partial f_{n,t}\left(\boldsymbol{p}_n^t,\zeta_{n,t}\right)}{\partial\zeta_{n,t}}=0. \tag{32}$$

Note that with fixed $\{\zeta_{n,t}, t\in\mathcal{M}, n\in\mathcal{N}\}$, (29) is convex, which is equivalent to (28) and can be solved by the interior-point method. By alternately updating $\{\zeta_{n,t}, t\in\mathcal{M}, n\in\mathcal{N}\}$ with fixed $\{\boldsymbol{P}_t, t\in\mathcal{M}\}$ and updating $\{\boldsymbol{P}_t, t\in\mathcal{M}\}$ with fixed $\{\zeta_{n,t}, t\in\mathcal{M}, n\in\mathcal{N}\}$, we run the iteration until triggering *Stop Condition 2*, which can be set as the maximum iteration number being reached. Then we obtain a solution of $\boldsymbol{p}_n^t$ as

$$\overrightarrow{\boldsymbol{p}}_n^t=\arg\max_{\boldsymbol{p}_n^t}\sum_{n=1}^{N_s}\sum_{t=1}^{M}f_{n,t}\left(\boldsymbol{p}_n^t,\zeta_{n,t}\right). \tag{33}$$

Therefore, given $\widehat{\boldsymbol{X}}$, we can obtain $\overrightarrow{\boldsymbol{p}}_n^t,\ t=1,2,\ldots,M$, based on the procedures from (28) to (33). Then the designed FDBF matrix given $\widehat{\boldsymbol{X}}$ is denoted as

$$\overrightarrow{\boldsymbol{P}}_t\triangleq[\overrightarrow{\boldsymbol{p}}_1^t,\overrightarrow{\boldsymbol{p}}_2^t,\ldots,\overrightarrow{\boldsymbol{p}}_{N_s}^t]. \tag{34}$$

For the illumination pattern design subproblem, given $\overrightarrow{\boldsymbol{P}}_1,\overrightarrow{\boldsymbol{P}}_2,\ldots,\overrightarrow{\boldsymbol{P}}_M$, (13) can be rewritten as

$$\max_{\widehat{\boldsymbol{X}}}\sum_{n=1}^{N_s}\sum_{t=1}^{M}R_{n,t}\left(\overrightarrow{\boldsymbol{P}}_t,\widehat{\boldsymbol{X}}\right) \tag{35a}$$

$$\text{s.t.}\quad\sum_{t=1}^{M}R_{n,t}\left(\overrightarrow{\boldsymbol{P}}_t,\widehat{\boldsymbol{X}}\right)\geqslant\gamma_n,\forall n\in\mathcal{N}, \tag{35b}$$

$$\sum_{n=1}^{N_s}x_{n,t}\leqslant K,\forall t\in\mathcal{M}, \tag{35c}$$

$$x_{n,t}\in\{0,1\},\forall n\in\mathcal{N},\forall t\in\mathcal{M}. \tag{35d}$$

Note that (35) is non-convex because of the logarithmic-fractional form of the objective function (35a) and the constraint (35b). To deal with the non-convexity of (35), we define an auxiliary variable as

$$\xi_{n,t}\triangleq\frac{\sqrt{\widehat{x}_{n,t}}\boldsymbol{h}_n^{\mathrm{H}}\overrightarrow{\boldsymbol{p}}_n^t}{\sum_{k\neq n}\widehat{x}_{k,t}\boldsymbol{h}_n\check{\boldsymbol{P}}_k^t\boldsymbol{h}_n^{\mathrm{H}}+\sigma^2}, \tag{36}$$

where

$$\check{\boldsymbol{P}}_k^t\triangleq\overrightarrow{\boldsymbol{p}}_k^t\left(\overrightarrow{\boldsymbol{p}}_k^t\right)^{\mathrm{H}},k\in\mathcal{N}. \tag{37}$$

Then we define two vectors $\boldsymbol{v}_n^t\in\mathbb{C}^{MN_s}$ and $\boldsymbol{d}_n^t\in\mathbb{C}^{MN_s}$ respectively as

$$\boldsymbol{v}_n^t\triangleq 2\mathrm{Re}\left\{\xi_{n,t}^{\mathrm{H}}\boldsymbol{h}_n\overrightarrow{\boldsymbol{p}}_n^t\right\}\boldsymbol{e}_M^t\otimes\boldsymbol{e}_{N_s}^n, \tag{38}$$

$$\boldsymbol{d}_n^t\triangleq\boldsymbol{e}_M^t\otimes\widehat{\boldsymbol{d}}_n^t, \tag{39}$$

where $\boldsymbol{e}_M^t$ denotes an M-dimensional column vector with its entries all being zero except its tth entry being one, $\boldsymbol{e}_{N_s}^n$ denotes an N_s-dimensional column vector with its entries all being zero except its nth entry being one, and the ith entry of $\widehat{\boldsymbol{d}}_n^t$ is

$$\left[\widehat{\boldsymbol{d}}_n^t\right]_i\triangleq\begin{cases}\boldsymbol{h}_n\check{\boldsymbol{P}}_k^t\boldsymbol{h}_n^{\mathrm{H}}, & i\in\mathcal{N},i\neq k,\\ 0, & i=k.\end{cases} \tag{40}$$

To give compact notation, we stack the relaxed continuous variables together as

$$\widehat{\boldsymbol{x}}_t\triangleq[\widehat{x}_{1,t},\widehat{x}_{2,t},\ldots,\widehat{x}_{N_s,t}]^{\mathrm{T}}, \tag{41}$$

$$\boldsymbol{x}\triangleq\left[\widehat{\boldsymbol{x}}_1^{\mathrm{T}},\widehat{\boldsymbol{x}}_2^{\mathrm{T}},\ldots,\widehat{\boldsymbol{x}}_M^{\mathrm{T}}\right]^{\mathrm{T}}. \tag{42}$$

Based on the quadratic transform, the achievable rate in (35a) can be expressed as

$$\begin{aligned}R_{n,t}(\overrightarrow{\boldsymbol{P}}_t,\widehat{\boldsymbol{X}})&=\log_2\left(1+\sqrt{\boldsymbol{x}}^{\mathrm{T}}\boldsymbol{v}_n^t-\xi_{n,t}^{\mathrm{H}}\left(\boldsymbol{x}^{\mathrm{T}}\boldsymbol{d}_n^t+\sigma^2\right)\xi_{n,t}\right)\\&\triangleq g_{n,t}\left(\xi_{n,t},\boldsymbol{x}\right),\end{aligned} \tag{43}$$

where $\sqrt{\boldsymbol{x}}$ is a vector with the same dimension as $\boldsymbol{x}$ and each entry of $\sqrt{\boldsymbol{x}}$ is the square root of that of $\boldsymbol{x}$, and $g_{n,t}\left(\xi_{n,t},\boldsymbol{x}\right)$ is a newly defined function. In fact, $\xi_{n,t}$ in (36) can be obtained by setting

$$\frac{\partial g_{n,t}\left(\xi_{n,t},\boldsymbol{x}\right)}{\partial\xi_{n,t}}=0. \tag{44}$$

Then (35) can be transformed into

$$\max_{\boldsymbol{x},\{\xi_{n,t},n\in\mathcal{N},t\in\mathcal{M}\}}\sum_{n=1}^{N_s}\sum_{t=1}^{M}g_{n,t}\left(\xi_{n,t},\boldsymbol{x}\right) \tag{45a}$$

$$\text{s.t.}\quad\sum_{t=1}^{M}g_{n,t}\left(\xi_{n,t},\boldsymbol{x}\right)\geqslant\gamma_n, \tag{45b}$$

$$\left(\boldsymbol{I}_M\otimes\boldsymbol{1}_{N_s}^{\mathrm{T}}\right)\boldsymbol{x}\preceq K\cdot\boldsymbol{1}_M, \tag{45c}$$

$$\boldsymbol{A}\boldsymbol{x}\succeq\boldsymbol{1}_{N_s}, \tag{45d}$$

where $\boldsymbol{A}\triangleq[\boldsymbol{I}_{N_s},\boldsymbol{I}_{N_s},\ldots,\boldsymbol{I}_{N_s}]\in\mathbb{R}^{N_s\times MN_s}$, $\boldsymbol{1}_{N_s}$ and $\boldsymbol{1}_M$ denote the N_s-dimensional and M-dimensional column vector with its entries all being one, respectively.

Note that with fixed $\{\xi_{n,t}, n\in\mathcal{N}, t\in\mathcal{M}\}$, (45) is convex, which can be solved by the existing convex optimization tools. By alternately updating $\{\xi_{n,t}, n\in\mathcal{N}, t\in\mathcal{M}\}$ with a fixed $\boldsymbol{x}$ and updating $\boldsymbol{x}$ with fixed $\{\xi_{n,t}, n\in\mathcal{N}, t\in\mathcal{M}\}$, we run the iterations until triggering *Stop Condition 3*, which can be set as the maximum iteration number being reached. The computational complexity of solving (45) is $O\left(T_3(MN_s)^{3.5}\log_2\left(1/\varepsilon_2\right)\right)$, where T_3 denotes the pre-defined maximum iteration number of *Stop Condition 3* and $\varepsilon_2>0$ is the solution accuracy of the CVX solver [24].

Based on the solutions of the FDBF design subproblem and illumination pattern design subproblem, now we propose an FDBF-IPAO scheme for the fully-digital BIP design problem by alternately optimizing these two subproblems until a stop condition is triggered.

Specifically, we initialize a feasible $\boldsymbol{x}$ by setting all its entries being K/N_s to satisfy (45c) and (45d), i.e.,

$$[\boldsymbol{x}]_i=K/N_s,\ i=1,2,\ldots,MN_s. \tag{46}$$

Algorithm 2 FDBF-IPAO Scheme

Input: N_{s}, N_{BS}, K, M.
Initialization: Initialize $\boldsymbol{x}$ via (46).
repeat
  repeat
    Update $\{\zeta_{n,t}, t \in \mathcal{M}, n \in \mathcal{N}\}$ via (31).
    Obtain $\{\boldsymbol{P}_t, t \in \mathcal{M}\}$ by solving (28).
  until *Stop Condition 2* is triggered
  Obtain $\overrightarrow{\boldsymbol{P}}_1, \overrightarrow{\boldsymbol{P}}_2, \ldots, \overrightarrow{\boldsymbol{P}}_M$ via (34).
  repeat
    Update $\{\xi_{n,t}, t \in \mathcal{M}, n \in \mathcal{N}\}$ via (36).
    Obtain $\boldsymbol{x}$ by solving (45).
  until *Stop Condition 3* is triggered
until *Stop Condition 4* is triggered
Obtain $\widetilde{\boldsymbol{X}}$ via (47).
Substitute $\widehat{\boldsymbol{X}}$ in (28) by $\widetilde{\boldsymbol{X}}$ and then solve (28), obtaining $\overrightarrow{\boldsymbol{P}}_1, \overrightarrow{\boldsymbol{P}}_2, \ldots, \overrightarrow{\boldsymbol{P}}_M$.
Output: $\overrightarrow{\boldsymbol{P}}_1, \overrightarrow{\boldsymbol{P}}_2, \ldots, \overrightarrow{\boldsymbol{P}}_M$, $\widetilde{\boldsymbol{X}}$.

Given $\boldsymbol{x}$, we update $\{\zeta_{n,t}, t \in \mathcal{M}, n \in \mathcal{N}\}$ via (31) and then obtain $\{\boldsymbol{P}_t, t \in \mathcal{M}\}$ by solving (28), which is indicated by step 4 to step 7 and is iteratively executed until triggering *Stop Condition 2*. Then we obtain $\overrightarrow{\boldsymbol{P}}_1, \overrightarrow{\boldsymbol{P}}_2, \ldots, \overrightarrow{\boldsymbol{P}}_M$ via (34). Based on the obtained $\overrightarrow{\boldsymbol{P}}_1, \overrightarrow{\boldsymbol{P}}_2, \ldots, \overrightarrow{\boldsymbol{P}}_M$, we updated $\{\xi_{n,t}, t \in \mathcal{M}, n \in \mathcal{N}\}$ via (36) and then obtain $\boldsymbol{x}$ by solving (45), which is indicated by step 9 to step 12 and is iteratively performed until triggering *Stop Condition 3*. We alternately run the above steps until triggering *Stop Condition 4*, which can be simply set that a predefined maximum number of iteration is reached. In fact, *Stop Condition 4* can be more effectively set that the objective of (28) can no longer increase.

To satisfy (35d), we need to quantize the continuous variables into binary ones by

$$\left[\widetilde{\boldsymbol{X}}\right]_{n,t} = \lfloor \boldsymbol{x}_{n+N_{\mathrm{s}}(t-1)} + 0.5 \rfloor. \tag{47}$$

If $\sum_{i=1}^{N_{\mathrm{s}}} \left[\widetilde{\boldsymbol{X}}\right]_{i,t} > K, t \in \mathcal{M}$, we define $\left[\widetilde{\boldsymbol{X}}\right]_{n,t} = \boldsymbol{x}_{n+N_{\mathrm{s}}(t-1)}$ and set the largest K entries in the tth column of $\widetilde{\boldsymbol{X}}$ as 1. Then, we achieve the designed illumination pattern $\widetilde{\boldsymbol{X}}$. Then we substitute $\widehat{\boldsymbol{X}}$ in (28) by $\widetilde{\boldsymbol{X}}$ and then solve (28), obtaining $\overrightarrow{\boldsymbol{P}}_1, \overrightarrow{\boldsymbol{P}}_2, \ldots, \overrightarrow{\boldsymbol{P}}_M$ as the finally designed fully-digital beamformers.

The detailed steps of the proposed FDBF-IPAO scheme are summarized in **Algorithm 2**. The computational complexity of FDBF-IPAO scheme is $O\big(\left((T_4+1)\,T_2 N_{\mathrm{BS}}^{3.5} + T_4 T_3\right)(M N_{\mathrm{s}})^{3.5} \log_2(1/\varepsilon_2)\big)$, where T_2 and T_4 denote the maximum iteration numbers of *Stop Condition 2* and *Stop Condition 4*, respectively.

C. HBF-AM Algorithm

Based on the FDBF matrices $\widetilde{\boldsymbol{P}}_1, \widetilde{\boldsymbol{P}}_2, \ldots, \widetilde{\boldsymbol{P}}_M$ designed by the FDBF-IPRS scheme or $\overrightarrow{\boldsymbol{P}}_1, \overrightarrow{\boldsymbol{P}}_2, \ldots, \overrightarrow{\boldsymbol{P}}_M$ designed by the FDBF-IPAO scheme, now we determine the hybrid beamformers, which are essentially the multiplication of the analog beamformers and digital beamformers. Without loss of generality, we use the designed FDBF matrices $\widetilde{\boldsymbol{P}}_1, \widetilde{\boldsymbol{P}}_2, \ldots, \widetilde{\boldsymbol{P}}_M$ to present the HBF-AM algorithm.

By minimizing the Euclidean distance between the designed fully-digital beamformers and the hybrid beamformers, the HBF design problem for $t = 1, 2, \ldots, M$ can be expressed as

$$\min_{\boldsymbol{F}_t, \boldsymbol{Q}_t} \ \left\|\widetilde{\boldsymbol{P}}_t - \boldsymbol{F}_t \boldsymbol{Q}_t\right\|_{\mathrm{F}} \tag{48a}$$

$$\text{s.t.} \quad \left\|\boldsymbol{F}_t \boldsymbol{Q}_t\right\|_{\mathrm{F}}^2 \leqslant P_{\mathrm{tot}}, \tag{48b}$$

$$\left|[\boldsymbol{F}_t]_{i,n}\right| = 1, \forall i \in \mathcal{N}_{\mathrm{BS}}, n \in \mathcal{N}, \tag{48c}$$

where (48b) is the total transmission power constraint and (48c) is the unit-modulus constraint due to the phase shifters in analog beamformers. In fact, we can temporarily neglect (48b) to solve the following problem as

$$\min_{\boldsymbol{F}_t, \boldsymbol{Q}_t} \ \left\|\widetilde{\boldsymbol{P}}_t - \boldsymbol{F}_t \boldsymbol{Q}_t\right\|_{\mathrm{F}} \tag{49a}$$

$$\text{s.t.} \quad \left|[\boldsymbol{F}_t]_{i,n}\right| = 1, \forall i \in \mathcal{N}_{\mathrm{BS}}, n \in \mathcal{N}. \tag{49b}$$

Note that (48b) can be satisfied via normalizing $\boldsymbol{Q}_t$ obtained from (49). For (49), the analog beamformers $\boldsymbol{F}_t$ and digital beamformers $\boldsymbol{Q}_t$ can be designed by alternately performing the following two steps.

- *Step 1:* Given a feasible solution of $\boldsymbol{F}_t$ denoted as $\widehat{\boldsymbol{F}}_t$, the digital beamformer design problem can be formulated as

$$\min_{\boldsymbol{Q}_t} \ \left\|\widetilde{\boldsymbol{P}}_t - \boldsymbol{F}_t \boldsymbol{Q}_t\right\|_{\mathrm{F}} \tag{50}$$

  which can be solved by the least squared method with the solution as

$$\widehat{\boldsymbol{Q}}_t = \left(\boldsymbol{F}_t^{\mathrm{H}} \boldsymbol{F}_t\right)^{-1} \boldsymbol{F}_t^{\mathrm{H}} \widetilde{\boldsymbol{P}}_t. \tag{51}$$

- *Step 2:* Given $\widehat{\boldsymbol{Q}}_t$, the analog beamformer design problem can be formulated as

$$\min_{\boldsymbol{F}_t} \ \left\|\widetilde{\boldsymbol{P}}_t - \boldsymbol{F}_t \widehat{\boldsymbol{Q}}_t\right\|_{\mathrm{F}} \tag{52a}$$

$$\text{s.t.} \quad \left|[\boldsymbol{F}_t]_{i,n}\right| = 1, \forall i \in \mathcal{N}_{\mathrm{BS}}, n \in \mathcal{N}, \tag{52b}$$

  which can be solved by the Riemannian manifold optimization method using the existing toolbox.

We iteratively perform the above two steps until *Stop Condition 5* is triggered, which can be set as the maximum iteration number being reached. For the obtained $\widehat{\boldsymbol{Q}}_t$ and $\widehat{\boldsymbol{F}}_t$ after finishing all the iterations, we normalize $\widehat{\boldsymbol{Q}}_t$ to satisfy (48b) via

$$\widehat{\boldsymbol{Q}}_t \leftarrow \frac{\sqrt{P_{\mathrm{tot}}}}{\left\|\widehat{\boldsymbol{F}}_t \widehat{\boldsymbol{Q}}_t\right\|_{\mathrm{F}}} \widehat{\boldsymbol{Q}}_t. \tag{53}$$

We repeat the same procedure for $t = 1, 2, \ldots, M$ and obtain the analog beamformers $\widehat{\boldsymbol{F}}_1, \widehat{\boldsymbol{F}}_2, \ldots, \widehat{\boldsymbol{F}}_M$ and digital beamformers $\widehat{\boldsymbol{Q}}_1, \widehat{\boldsymbol{Q}}_2, \ldots, \widehat{\boldsymbol{Q}}_M$.

The detailed steps for the HBF-AM algorithm are summarized in **Algorithm 3**. Note that the computational complexity of the HBF-AM algorithm is $O\big(M T_5 \left(N_{\mathrm{s}}^3 + N_{\mathrm{BS}} N_{\mathrm{s}}\right)\big)$, where T_5 denotes the predefined maximum iteration number of *Stop Condition 5*.

Algorithm 3 HBF-AM Algorithm

Input: $\widetilde{\boldsymbol{P}}_1, \widetilde{\boldsymbol{P}}_2, \ldots, \widetilde{\boldsymbol{P}}_M$
for $t = 1, 2, \ldots, M$ **do**
  repeat
    Randomly generate $\boldsymbol{F}_t$ based on (48c).
    Compute $\widehat{\boldsymbol{Q}}_t$ via (51).
    Obtain $\widehat{\boldsymbol{F}}_t$ by solving (52).
  until *Stop Condition 5* is triggered
  Normalized $\widehat{\boldsymbol{Q}}_t$ via (53).
end for
Output: $\widehat{\boldsymbol{F}}_1, \widehat{\boldsymbol{F}}_2, \ldots, \widehat{\boldsymbol{F}}_M$ and $\widehat{\boldsymbol{Q}}_1, \widehat{\boldsymbol{Q}}_2, \ldots, \widehat{\boldsymbol{Q}}_M$.

To solve the joint BIP problem in (11), if we use the FDBF-IPRS scheme followed by the HBF-AM algorithm, the computational complexity is

$$O\left(IT_1(MN_{\mathrm{BS}}N_{\mathrm{s}})^{3.5}\log_2(1/\varepsilon_1) + MT_5\left(N_{\mathrm{s}}^3 + N_{\mathrm{BS}}N_{\mathrm{s}}\right)\right). \tag{54}$$

If we use the FDBF-IPAO scheme followed by the HBF-AM algorithm, the computational complexity is

$$O\Big(\left((T_4+1)T_2{N_{\mathrm{BS}}}^{3.5} + T_4T_3\right)(MN_{\mathrm{s}})^{3.5}\log_2\left(1/\varepsilon_2\right) + MT_5\left(N_{\mathrm{s}}^3 + N_{\mathrm{BS}}N_{\mathrm{s}}\right)\Big). \tag{55}$$

Since the computational complexity to determine the fully-digital beamformers given the illumination pattern based on the FP method is similar for the FDBF-IPRS and FDBF-IPAO schemes, T_1 and T_2 are similar. To find a near-optimal solution from the randomly generated illumination pattern, I needs to be set large, where I is typically much larger than T_4. To be specific, we set

$$I = \frac{1}{M!}\underbrace{C_{N_{\mathrm{s}}}^{K}C_{N_{\mathrm{s}}-K}^{K}\cdots C_{N_{\mathrm{s}}-(M-1)K}^{K}}_{M}, \tag{56}$$

where $C_{N_{\mathrm{s}}}^{K}$ denotes the binomial coefficient of choosing K beam positions from the total N_{s} beam positions. It is seen that as N_{s} becomes large, I gets extremely large. Therefore, the computational complexity of FDBF-IPRS is much higher than that of FDBF-IPAO. On the other hand, as I grows to be infinity, the optimal solution will be obtained by FDBF-IPRS.

IV. Simulation Results

We assume that the LEO satellite is equipped with $N_{\mathrm{BS}} = 64$ antennas, $N_{\mathrm{RF}} = 6$ RF chains and $N_{\mathrm{s}} = 6$ beam positions, where the maximum number of illuminated beam positions is $K = 2$ and the number of BH time slots is $M = 3$. The channels between the LEO satellite and each beam position are supposed to include $L_n = 2$ channel paths, where the channel gain $g_l^{(n)}$ obeys Rician fading distribution with Rician factor $\chi_l^{(n)} = 10$ dB. The simulation parameters are mainly summarized in Table I. Note that in this paper the HBF design is performed by the HBF-AM algorithm, based on the FDBF designed by either the FDBF-IPRS or FDBF-IPAO scheme. For simplicity, we set $N_{\mathrm{s}} = KM$. In fact, if N_{s} cannot be evenly divided by M or K, we suppose $N_{\mathrm{s}} = KM + D$, where N_{s} is divided by K with a remainder D. Then we need $M+1$ time slots, where D beam positions are illuminated in one time slot and K beam positions are illuminated in each of the M time slots.

TABLE I
Simulation Parameters

Parameter	Value
Numbers of satellite antennas N_{BS}	64
Numbers of total beam positions N_{s}	6
Numbers of time slots M	3
Rician factor $\chi_l^{(n)}$	10 dB
Bandwidth B	250 MHz
Carrier frequency f_c	20 GHz
Boltzmann's constant κ	$1.38 \times 10^{-23}\mathrm{J}\cdot\mathrm{K}^{-1}$
Receiving noise temperature T_{R}	293 K

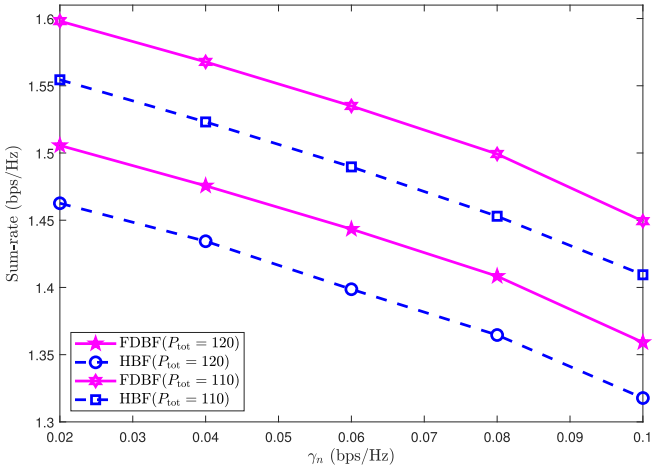

Fig. 2. Comparisons of sum-rate of total N_{s} beam positions under different γ_n for FDBF design and HBF design with different P_{tot}.

As shown in Fig. 2, we compare the sum-rate of total N_{s} beam positions under different γ_n and P_{tot} with fixed $N_{\mathrm{BS}} = 64$ and $N_{\mathrm{s}} = 6$, where the FDBF-IPRS scheme is employed for both the FDBF and HBF design. For simplicity, γ_n is set the same for different n. It is observed that as γ_n increases, the sum-rate of total N_{s} beam positions falls, which implies that a high requirement of the sum-rate from the individual beam position results in a poor sum-rate of the total beam positions. When P_{tot} grows from 110 to 120 W, the sum-rate can be increased by around 10% for either FDBF and HBF given the same γ_n.

As shown in Fig. 3, we compare the sum-rate of total N_{s} beam positions under different γ_n and N_{BS} with fixed $N_{\mathrm{s}} = 6$ and $P_{\mathrm{tot}} = 120$ W, where the FDBF-IPRS scheme is employed for both the FDBF and HBF design. For simplicity, we set γ_n the same for different n. It can be observed that the sum-rate of total N_{s} beam positions falls as γ_n increases. For both FDBF and HBF with the same γ_n, a larger antenna array provides more beamforming design degrees of freedom.

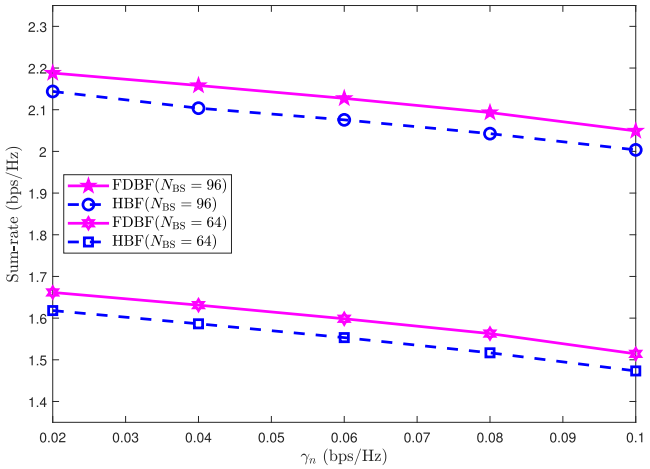

Fig. 3. Comparisons of sum-rate of total N_s beam positions under different N_{BS} for FDBF design and HBF design with different γ_n.

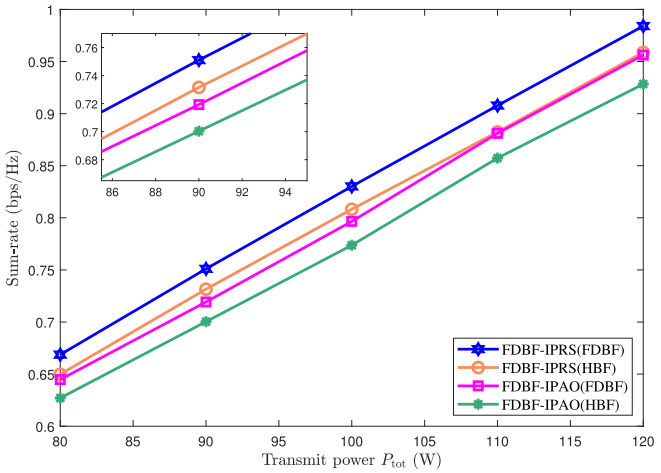

Fig. 5. Comparisons of sum-rate of FDBF-IPRS and FDBF-IPAO schemes under different P_{tot}.

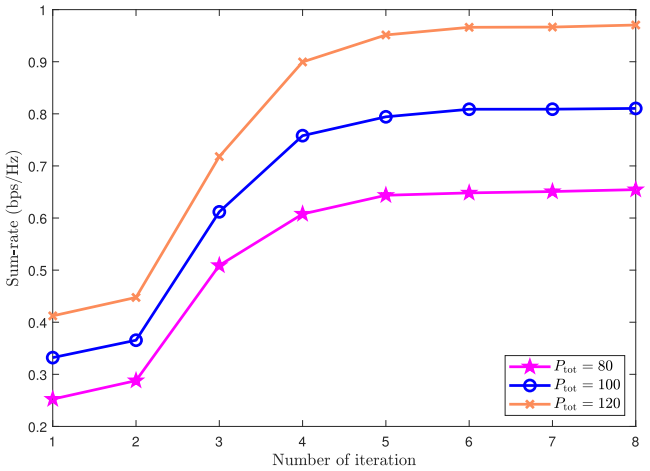

Fig. 4. Convergence of the sum-rate of FDBF-IPAO scheme with different P_{tot}.

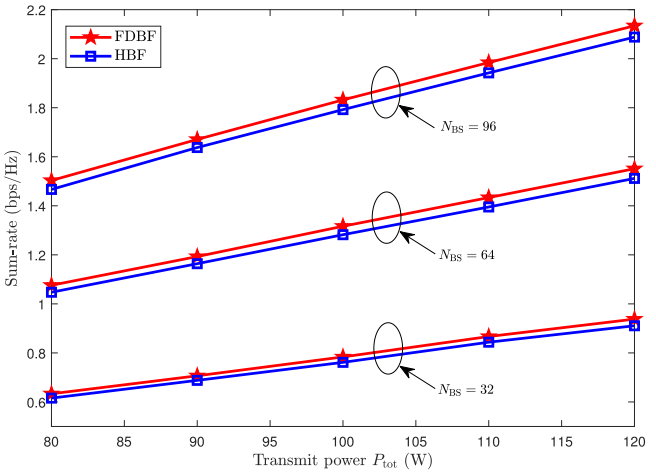

Fig. 6. Comparisons of sum-rate of total N_s beam positions under different P_{tot} for FDBF and HBF equipped with different N_{BS}.

When increasing from $N_{BS}=64$ to $N_{BS}=96$, the sum-rate can be improved by around 33%.

To evaluate the convergence of the FDBF-IPAO scheme, we provide the sum-rate versus the number of iterations for different P_{tot}, as shown in Fig. 4. We set $\gamma_n=0.01$ bps/Hz, $N_{BS}=32$ and $N_s=6$. When P_{tot} grows from 80 to 120 W, the sum-rate can be increased from 0.65 bps/Hz to 0.97 bps/Hz with 50% improvement. Moreover, it can be seen that the FDBF-IPAO scheme can converge in no more than eight iterations.

As shown in Fig. 5, we compare the sum-rate under different P_{tot} for FDBF and HBF with fixed $\gamma_n=0.01$ bps/Hz, $N_{BS}=32$ and $N_s=6$, where different schemes including FDBF-IPRS and FDBF-IPAO are employed. It can be observed that as P_{tot} increase, the sum-rate of total N_s beam positions increases for both FDBF and HBF. For either FDBF-IPRS or FDBF-IPAO, the sum-rate of HBF is lower than that of FDBF, since HBF has constraints from the phase shifter networks and achieves lower hardware complexity than FDBF. For the same FDBF, the sum-rate achieved by the FDBF-IPAO scheme is slightly lower than that achieved by the FDBF-IPRS scheme. The reason is that the FDBF-IPAO scheme reduces the computational complexity by solving the continuous optimization problem for illumination pattern design, where the random initialization of the illumination pattern may lead to a fast convergence to a locally optimal solution.

Fig. 6 compares the sum-rate of total N_s beam positions for FDBF and HBF using the FDBF-IPAO scheme, where we set different P_{tot} and N_{BS} and fix $\gamma_n=0.01$ bps/Hz. It is seen that larger P_{tot} leads to higher sum-rate. To further evaluate the impact of different antenna numbers, we set $N_{BS}=32$, 64 and 96 for both FDBF and HBF design schemes. When we enlarge N_{BS} from 32 to 96, the increased sum-rate can be achieved for the same P_{tot}. Furthermore, as N_{BS} increases, the gap between FDBF and HBF becomes large. The reason is that more antennas lead to more unit-modulus constraints coming from the phase shifters for HBF, which makes HBF more difficult to approach the performance of FDBF.

As shown in Fig. 7, we compare the sum-rate for different K and M using the FDBF-IPAO scheme for the HBF design. We fix $\gamma_n=0.01$ bps/Hz and $N_{BS}=32$. In fact, we compare $N_s=4$, $N_s=6$ and $N_s=8$. It is seen that as N_s increases, the sum-rate substantially improves. When fixing $K=2$, either enlarging $M=2$ to $M=3$ or enlarging $M=3$ to $M=4$ leads to around 40% increase of the sum-rate, which implies that more time slots for SatComs

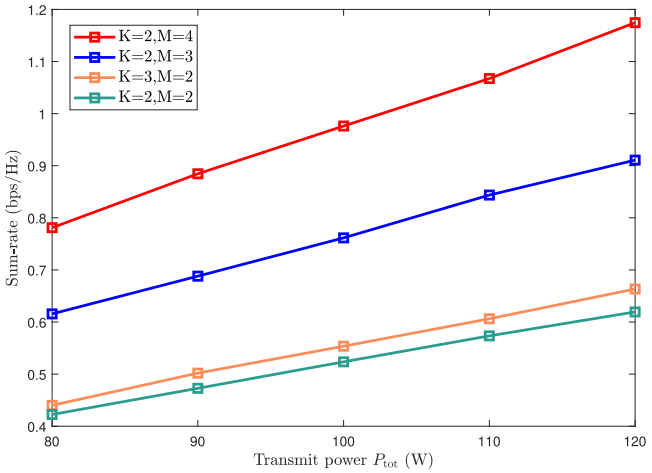

Fig. 7. Comparisons of sum-rate of total N_{s} beam positions for different K and M.

can effectively improve the sum-rate. When fixing $M = 2$, enlarging $K = 2$ to $K = 3$ leads to around 6% increase of the sum-rate. When fixing $N_{\text{s}} = 6$, the sum-rate of $K = 2$ and $M = 3$ is around 38% higher than that of $K = 3$ and $M = 2$, which implies that improving the number of time slots for SatComs is more effective than increasing the number of illuminated beam position within the same time slot.

V. Conclusion

In this paper, we have investigated the HBF design for BH LEO SatComs. Aiming at maximizing the sum-rate of totally illuminated beam positions during the whole BH period, we have considered the joint BIP design problem subject to the HBF constraints and sum-rate requirements. To solve this joint BIP design problem, we have temporarily replaced the HBF constraints with the FDBF constraints and converted the original problem into a fully-digital BIP design problem. We have proposed the FDBF-IPRS and FDBF-IPAO schemes to design the fully-digital beamformers. Then we have proposed the HBF-AM algorithm to design the hybrid beamformers. Simulation results have shown that the proposed schemes can achieve satisfactory sum-rate performance for BH LEO SatComs. Future work will be continued with the focus on the power allocation for BH LEO SatComs.

References

[1] J. Wang, C. Qi, and S. Yu, "Hybrid beamforming design for beam-hopping LEO satellite communications," in *Proc. IEEE Global Commun. Conf.*, Kuala Lumpur, Malaysia, Dec. 2023, pp. 3959–3964.

[2] O. Kodheli et al., "Satellite communications in the new space era: A survey and future challenges," *IEEE Commun. Surveys Tuts.*, vol. 23, no. 1, pp. 70–109, 1st Quart., 2021.

[3] C. Qi, J. Wang, L. Lyu, L. Tan, J. Zhang, and G. Y. Li, "Key issues in wireless transmission for NTN-assisted Internet of Things," *IEEE Internet Things Mag.*, vol. 7, no. 1, pp. 40–46, Jan. 2024.

[4] Z. Xiao et al., "LEO satellite access network (LEO-SAN) towards 6G: Challenges and approaches," *IEEE Wireless Commun.*, vol. 31, no. 2, pp. 89–96, Apr. 2024.

[5] X. Lin, S. Cioni, G. Charbit, N. Chuberre, S. Hellsten, and J. Boutillon, "On the path to 6G: Embracing the next wave of low earth orbit satellite access," *IEEE Commun. Mag.*, vol. 59, no. 12, pp. 36–42, Dec. 2021.

[6] I. del Portillo, B. G. Cameron, and E. F. Crawley, "A technical comparison of three low earth orbit satellite constellation systems to provide global broadband," *Acta Astronautica*, vol. 159, pp. 123–135, Jun. 2019.

[7] L. Lyu and C. Qi, "Beam position and beam hopping design for LEO satellite communications," *China Commun.*, vol. 20, no. 7, pp. 29–42, Jul. 2023.

[8] V. N. Ha, T. T. Nguyen, E. Lagunas, J. C. Merlano Duncan, and S. Chatzinotas, "GEO payload power minimization: Joint precoding and beam hopping design," in *Proc. IEEE Global Commun. Conf. (GLOBECOM)*, Rio de Janeiro, Brazil, Sep. 2022, pp. 6445–6450.

[9] L. Chen, V. N. Ha, E. Lagunas, L. Wu, S. Chatzinotas, and B. Ottersten, "The next generation of beam hopping satellite systems: Dynamic beam illumination with selective precoding," *IEEE Trans. Wireless Commun.*, vol. 22, no. 4, pp. 2666–2682, Apr. 2023.

[10] A. Wang, L. Lei, E. Lagunas, A. I. Pérez-Neira, S. Chatzinotas, and B. Ottersten, "Joint optimization of beam-hopping design and NOMA-assisted transmission for flexible satellite systems," *IEEE Trans. Wireless Commun.*, vol. 21, no. 10, pp. 8846–8858, Oct. 2022.

[11] T. Li, R. Yao, Y. Fan, X. Zuo, N. I. Miridakis, and T. A. Tsiftsis, "Pattern design and power management for cognitive LEO beaming hopping satellite-terrestrial networks," *IEEE Trans. Cogn. Commun. Netw.*, vol. 9, no. 6, pp. 1531–1545, Dec. 2023.

[12] Q. Gao, M. Jia, Q. Guo, X. Gu, and L. Hanzo, "Jointly optimized beamforming and power allocation for full-duplex cell-free NOMA in space-ground integrated networks," *IEEE Trans. Commun.*, vol. 71, no. 5, pp. 2816–2830, May 2023.

[13] H. Zhou, J. Li, K. Yang, H. Zhou, J. An, and Z. Han, "Handover analysis in ultra-dense LEO satellite networks with beamforming methods," *IEEE Trans. Veh. Technol.*, vol. 72, no. 3, pp. 3676–3690, Mar. 2023.

[14] C. Qi, Y. Yang, R. Ding, S. Jin, and D. Liu, "Multibeam satellite communications with energy efficiency optimization," *IEEE Commun. Lett.*, vol. 26, no. 4, pp. 887–891, Apr. 2022.

[15] L. You et al., "Hybrid analog/digital precoding for downlink massive MIMO LEO satellite communications," *IEEE Trans. Wireless Commun.*, vol. 21, no. 8, pp. 5962–5976, Aug. 2022.

[16] D. Peng, A. Bandi, Y. Li, S. Chatzinotas, and B. Ottersten, "Hybrid beamforming, user scheduling, and resource allocation for integrated terrestrial-satellite communication," *IEEE Trans. Veh. Technol.*, vol. 70, no. 9, pp. 8868–8882, Sep. 2021.

[17] T. Shi, Y. Liu, S. Kang, S. Sun, and R. Liu, "Angle-based multicast user selection and precoding for beam-hopping satellite systems," *IEEE Trans. Broadcast.*, vol. 69, no. 4, pp. 856–871, Dec. 2023.

[18] L. Zhu, W. Ma, and R. Zhang, "Movable antennas for wireless communication: Opportunities and challenges," *IEEE Commun. Mag.*, vol. 62, no. 6, pp. 114–120, Jun. 2024.

[19] L. Zhu, X. Pi, W. Ma, Z. Xiao, and R. Zhang, "Dynamic beam coverage for satellite communications aided by movable-antenna array," 2024, *arXiv:2404.15643*.

[20] C. Zhang, X. Zhao, and G. Zhang, "Joint precoding schemes for flexible resource allocation in high throughput satellite systems based on beam hopping," *China Commun.*, vol. 18, no. 9, pp. 48–61, Sep. 2021.

[21] H. Yang, D. Yang, Y. Li, and J. Kuang, "Cluster-based beam hopping for energy efficiency maximization in flexible multibeam satellite systems," *IEEE Commun. Lett.*, vol. 27, no. 12, pp. 3300–3304, Dec. 2023.

[22] C. Qi, H. Chen, Y. Deng, and A. Nallanathan, "Energy efficient multicast precoding for multiuser multibeam satellite communications," *IEEE Wireless Commun. Lett.*, vol. 9, no. 4, pp. 567–570, Apr. 2020.

[23] K. Shen and W. Yu, "Fractional programming for communication systems—Part II: Uplink scheduling via matching," *IEEE Trans. Signal Process.*, vol. 66, no. 10, pp. 2631–2644, May 2018.

[24] M. Grant and S. Boyd. (Jun. 2009). *CVX: MATLAB Software for Disciplined Convex Programming*. [Online]. Available: http://stanford.edu/boyd/cvx

Jing Wang (Graduate Student Member, IEEE) received the B.S. degree in communication engineering from Nanjing Normal University, Nanjing, China, in 2019, and the M.E. degree in information and communication engineering from China University of Mining and Technology, Xuzhou, China, in 2022. She is currently pursuing the Ph.D. degree in information and communication engineering with the School of Information Science and Engineering, Southeast University, Nanjing. Her research interests include satellite communications and signal processing.

Chenhao Qi (Senior Member, IEEE) received the B.S. degree (Hons.) in information engineering from the Chien-Shiung Wu Honored College, Southeast University, China, in 2004, and the Ph.D. degree in signal and information processing from Southeast University, in 2010.

From 2008 to 2010, he visited the Department of Electrical Engineering, Columbia University, New York, NY, USA. Since 2010, he has been a Faculty Member with the School of Information Science and Engineering, Southeast University, where he is currently a Professor and the Head of Jiangsu Multimedia Communication and Sensing Technology Research Center. He received best paper awards from IEEE GLOBECOM in 2019, IEEE/CIC ICCC in 2022, and the 11th International Conference on Wireless Communications and Signal Processing (WCSP) in 2019. He served as an Associate Editor for IEEE TRANSACTIONS ON COMMUNICATIONS, IEEE COMMUNICATIONS LETTERS, IEEE OPEN JOURNAL OF THE COMMUNICATIONS SOCIETY, IEEE OPEN JOURNAL OF VEHICULAR TECHNOLOGY, and *China Communications*.

Shui Yu (Fellow, IEEE) received the Ph.D. degree from Deakin University, Australia, in 2004. He is currently a Professor with the School of Computer Science and the Deputy Chair of the University Research Committee, University of Technology Sydney, Australia. He has published five monographs and edited two books and more than 600 technical articles at different venues, such as IEEE TRANSACTIONS ON DEPENDABLE AND SECURE COMPUTING, IEEE TRANSACTIONS ON PARALLEL AND DISTRIBUTED SYSTEMS, IEEE TRANSACTIONS ON COMPUTERS, IEEE TRANSACTIONS ON INFORMATION FORENSICS AND SECURITY, IEEE TRANSACTIONS ON MOBILE COMPUTING, IEEE TRANSACTIONS ON KNOWLEDGE AND DATA ENGINEERING, IEEE TRANSACTIONS ON EMERGING TOPICS IN COMPUTING, IEEE/ACM TRANSACTIONS ON NETWORKING, and INFOCOM. His current H-index is 79. His research interests include cybersecurity, network science, big data, and mathematical modeling. He has been promoting the research field of networking for big data since 2013 and his research outputs have been widely adopted by industrial systems, such as Amazon cloud security. He is a member of ACM and AAAS. He is also serving on the editorial boards for IEEE COMMUNICATIONS SURVEYS AND TUTORIALS (Area Editor) and IEEE INTERNET OF THINGS JOURNAL (Editor). He served as a Distinguished Lecturer for the IEEE Communications Society (2018–2021). He is a Distinguished Visitor of the IEEE Computer Society and an Elected Member of the Board of Governors of IEEE VTS and ComSoc.

Shiwen Mao (Fellow, IEEE) received the Ph.D. degree in electrical engineering from Polytechnic University in 2004. He is currently a Professor, an Earle C. Williams Eminent Scholar, and the Director of the Wireless Engineering Research and Education Center, Auburn University. His research interests include wireless networks, multimedia communications, and smart grids. He received the IEEE ComSoc MMTC Outstanding Researcher Award in 2023, the SEC 2023 Faculty Achievement Award for Auburn, the IEEE ComSoc TC-CSR Distinguished Technical Achievement Award in 2019, Auburn University Creative Research and Scholarship Award in 2018, and the NSF CAREER Award in 2010, and several service awards from IEEE ComSoc. He was a co-recipient of the 2022 Best Journal Paper Award of IEEE ComSoc eHealth Technical Committee, the 2021 Best Paper Award of Elsevier/KeAi Digital Communications and Networks Journal, the 2021 IEEE Internet of Things Journal Best Paper Award, the 2021 IEEE Communications Society Outstanding Paper Award, the IEEE Vehicular Technology Society 2020 Jack Neubauer Memorial Award, the 2018 Best Journal Paper Award and the 2017 Best Conference Paper Award from IEEE ComSoc MMTC, and the 2004 IEEE Communications Society Leonard G. Abraham Prize in the Field of Communications Systems. He was a co-recipient of the best paper awards from IEEE GLOBECOM 2023 (two) 2019, 2016, and 2015, IEEE ICC 2022 and 2013, and IEEE WCNC 2015, and the best demo awards from IEEE INFOCOM 2024, IEEE INFOCOM 2022, and IEEE SECON 2017. He is the Editor-in-Chief of IEEE TRANSACTIONS ON COGNITIVE COMMUNICATIONS AND NETWORKING, a Member-at-Large of the IEEE Communications Society Board of Governors, and the Vice President of the Technical Activities of IEEE Council on Radio Frequency Identification (CRFID).